

Third order nonlinear transport properties in topological chiral antiferromagnetic semimetal CoNb_3S_6

Junjian Mi^{1,2#}, Jialin Li^{2,3#}, Miaocong Li¹, Sheng Xu¹, Shuang Yu¹, Zheng Li¹, Xinyi Fan², Huanfeng Zhu^{2,4}, Qian Tao¹, Linjun Li^{2*}, Zhuan Xu^{1,5,6*}

1. Zhejiang Province Key Laboratory of Quantum Technology and Device, School of Physics, Zhejiang University, Hangzhou 310027, China
2. State Key Laboratory of Modern Optical Instrumentation College of Optical Science and Engineering Zhejiang University, Hangzhou 310027, China
3. Hangzhou Institute for Advanced Study, University of Chinese Academy of Sciences, Hangzhou 310024, China
4. Jiaxing Key Laboratory of Photonic Sensing & Intelligent Imaging Jiaxing Institute Zhejiang University, Jiaxing 314000, China
5. State Key Laboratory of Silicon and Advanced Semiconductor Materials, Zhejiang University, Hangzhou 310027, China
6. Hefei National Laboratory, Hefei 230088, China

#These authors contributed equally to this work

*corresponding author. E-mail: lilinjun@zju.edu.cn; zhuan@zju.edu.cn

Abstract

The topology between Bloch states in reciprocal space has attracted tremendous attention in recent years. The quantum geometry of the band structure is composed of quantum metric as real part and berry curvature as imaginary part. While the Berry curvature, the Berry curvature dipole and Berry connection polarizability have been recently revealed by the first order anomalous hall, second order and third order nonlinear Hall effect respectively, the quantum metric induced second order nonlinear transverse and longitudinal response in topological antiferromagnetic material MnBi_2Te_4 was only very recently reported. Here we demonstrate the similar third order nonlinear transport properties in the topological antiferromagnetic CoNb_3S_6 . We observed that the third order nonlinear longitudinal V_{xx}^{3o} increase significantly at the antiferromagnetic transition temperature T_N

∩ 29 K, which was probably induced by the quantum metric without time-reversal symmetry or inversion symmetry. Besides, temperature-dependent nonlinear behaviour was observed in the first order I-V curve below the Neel temperature T_N , which was not reported in MnBi_2Te_4 and FeSn . Such nonlinear I-V behaviour hints for the possible existence of Charge Density Wave (CDW) state, which has been discovered in its sister material FeNb_3S_6 . Simultaneously, two plateaus in the third order nonlinear longitudinal $V_{xx}^{3\omega} \sim I^\omega$ curve are observed, which is also speculated to be related with the possible CDW state. However, the genuine mechanism for the first order nonlinear I-V and its relation with the third order nonlinear transport call for more experimental investigations and theoretical interpretation. Our work provides a way to explore third harmonic nonlinear transport and interaction with magnetic order and CDW.

Introduction

The intrinsic nonlinear hall responses are connected to topological properties of material, which have attracted tremendous interests in condensed materials physics in recent years^{1, 2, 3, 4, 5, 6, 7, 8, 9, 10, 11, 12, 13, 14, 15, 16, 17}. The Berry curvature and the quantum metric are the imaginal part and real part of the quantum geometric tensor, respectively. They and their differential derivatives have been unveiled to be responsible to the interesting nonlinear transport phenomenon. For instance, the Berry curvature induces the anomalous Hall effect (AHE)¹⁸. The Berry curvature dipole can lead to second order nonlinear Hall effect and the Berry connection polarizability can induce third order nonlinear Hall effect in non-magnetic topological materials^{1, 2, 19, 20, 21}. Recently, such second order nonlinear transport induced by the quantum metric dipole has been

theoretically predicted and experimentally verified in topological antiferromagnetic material MnBi_2Te_4 ^{22, 23, 24, 25}. It is worth noting that, the Berry curvature can only contribute to the transverse conduction in nonlinear transport. However, the quantum metric can contribute to the both longitudinal and transverse nonlinear conductivity. While the intrinsic contribution to the nonlinear transport is determined by the quantum geometric property, the extrinsic mechanism like Skew scattering and Side jump could also lead to nonlinear transport^{5, 10}. Therefore, it is interesting to explore nonlinear transport in topological material, especially to discover its intrinsic quantum geometric contribution and cautiously exclude the possible extrinsic effect.

Third order nonlinear hall effect induced by the Berry connection polarizability tensor have been observed in nonmagnetic materials $\text{T}_d\text{-MoTe}_2$ and TaIrTe_4 ^{19, 20}. Recent theoretical work predicted Berry connection polarizability tensor can survive in certain magnetic topological material without time-reversal symmetry^{26, 27}. At the same time, we noticed that Ref^{28, 29} reported the quantum metric and Berry curvature induced third-order nonlinear transport phenomenon in topological antiferromagnetic material MnBi_2Te_4 and FeSn . Therefore, it is interesting to experimentally investigate the third nonlinear transport and their relation to the magnetic order. Therefore, we explore the third-order nonlinear transport in a topological antiferromagnetic semimetal CoNb_3S_6 , which has a previously theoretically predicted Berry connection polarizability tensor.

The large AHE and anomalous Nernst effect have been reported recently in CoNb_3S_6 ^{30, 31, 32}, which are probably induced by its intrinsic Berry curvature. The Weyl

points near the Fermi level were revealed by the Angle-resolved photoemission spectroscopy (ARPES) results and first-principle calculations were proposed for the cause of the large AHE^{33,34}. Besides, the all-in-all-out type non-coplanar antiferromagnetic (AFM) order have been proposed through polarized neutron scattering experiments³⁵. These interesting phenomena indicate CoNb₃S₆ is an attracting platform to investigate the interaction between its nonlinear transport properties and magnetic order.

In this work, we measured the third order nonlinear longitudinal $V_{xx}^{3\omega}$ and transverse $V_{xy}^{3\omega}$ signals driven by the a. c. current with frequency $\omega = 13.33$ Hz in high quality exfoliated CoNb₃S₆ single crystal. With the decrease of temperature, the third order nonlinear longitudinal $V_{xx}^{3\omega}$ increases significantly near the antiferromagnetic transition temperature ($T_N \sim 29$ K), and the $V_{xx}^{3\omega}$ decreases with further decrease of temperature. The sign of transverse $V_{xy}^{3\omega}$ has a change with part of contribution from longitudinal $V_{xx}^{3\omega}$ due to the asymmetry of the electrode. Surprisingly, the first order I-V curve behaves nonlinear characteristic below the Neel temperature T_N . Such first order nonlinear I-V behaviour possibly corresponds to a Charge Density Wave (CDW) gap along with the antiferromagnetic order transition, which bears similarity to its sister material FeNb₃S₆³⁶. Correspondingly, the third order nonlinear longitudinal $V_{xx}^{3\omega}$ -T curve has two plateaus with the amplitude of current increases which was not observed in MnBi₂Te₄ or other materials. The magnetic field-dependent third order nonlinear transverse $V_{xy}^{3\omega}$ undergoes a loop which is consistent with its first order anomalous hall effect. Such third order nonlinear anomalous hall effect and longitudinal behaviour

below the Neel temperature $T_N \sim 29$ K are probably induced by the Berry curvature and Quantum metric respectively, as uncovered in systems without inversion symmetry and time-reversal symmetry, such as MnBi_2Te_4 very recently²⁹.

Results

1. The significantly enhanced longitudinal third-harmonic nonlinear voltage $V_{xx}^{3\omega}$ at AFM transitional temperature:

The crystal structure of CoNb_3S_6 is presented in Fig. 1(a) with the space group of $P6_322$ where the Co atoms are inserted between the layers of 2H-NbS_2 . Fig. 1(b) shows the temperature dependence of magnetic susceptibility, measured under an applied magnetic field of 0.1T along c-direction, with field cooling (black line) and zero field cooling (red line). Antiferromagnetic transition $T_N \sim 29$ K is determined from the temperature dependence of magnetic susceptibility, which is consistent with the former experiment report³¹. The inset displays the optical image of single crystal CoNb_3S_6 which was synthesized by chemical vapor transport method as described in Methods. Fig. 1(c) and Fig. 1(d) show the temperature dependence of the longitudinal first harmonic V_{xx}^{ω} voltage and third-harmonic voltage $V_{xx}^{3\omega}$ from 2 K to 300 K with applied a. c. current of 1.80 mA with the frequency $f = 13.33$ Hz. The temperature dependence of the longitudinal first-harmonic shows a metallic behaviour with a kink near 28 K (T_N), which is smaller than the AFM transition $T_N \sim 29$ K in magnetic susceptibility measurements. The decreasing of AFM transition temperature of CoNb_3S_6 in Fig.1c is probably restrained by the large current which was further studied with different

amplitude of a. c. current as shown in Fig. 4. The inset shows the atomic force microscopy image of the device. Fig. 1(d) shows the temperature dependence of the third-harmonic voltage $V_{xx}^{3\omega}$ from 2 K to 300 K. A peak third harmonic voltage $V_{xx}^{3\omega}$ of 0.92 mV was obtained at 26.6 K. Inset shows the detailed longitudinal third harmonic voltage $V_{xx}^{3\omega}$ from 2 K to 40 K.

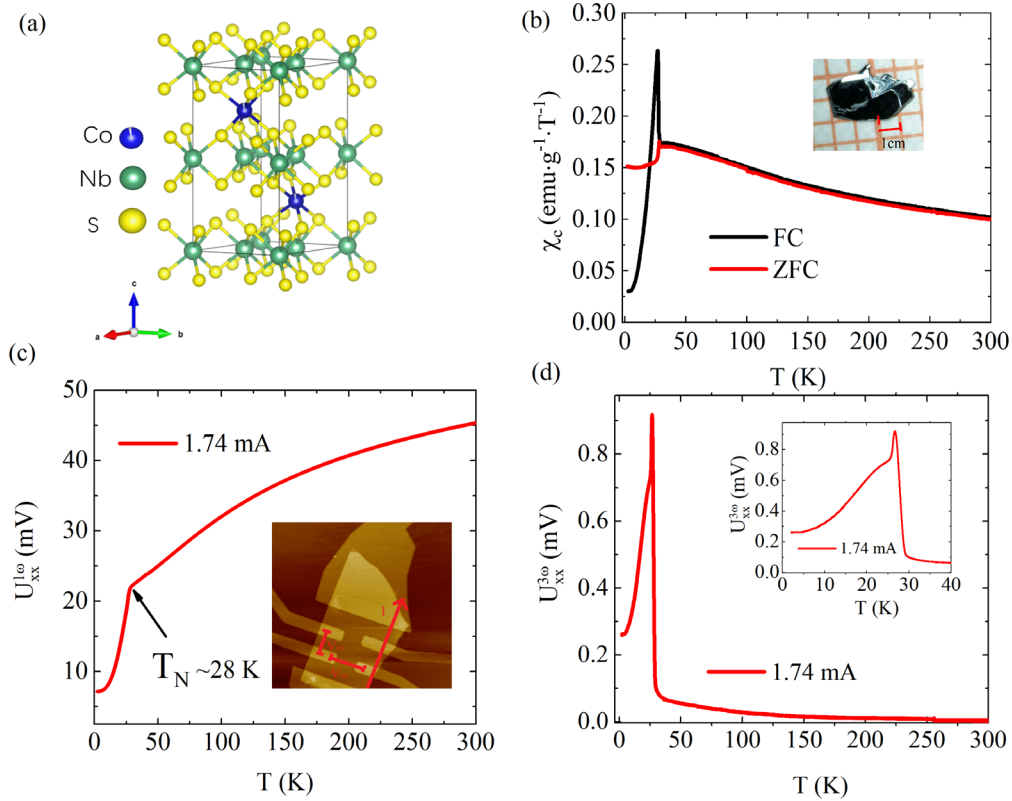


Fig. 1. Crystal structure, magnetic and electric transport properties of CoNb_3S_6 . (a) The crystal structure of CoNb_3S_6 . (b) Magnetic susceptibility measured with magnetic field along c-axis. Inset shows the optical image of as grown single crystal CoNb_3S_6 . (c) Temperature dependence of the longitudinal first harmonic voltage $V_{xx}^{1\omega}$ from 2 K to 300 K with applied a. c. current of 1.74 mA. Inset shows the atomic force microscopy image of the device used for electrical transport measurements, the sample thickness is about 100 nm. (d) Temperature dependence of the longitudinal third harmonic voltage $V_{xx}^{3\omega}$ from 2 K to 300 K with applied a. c. current of 1.74 mA.

Inset shows the longitudinal third harmonic voltage $V_{xx}^{3\omega}$ from 2 K to 40 K.

2. The magnetic field-dependent nonlinear transport properties in CoNb_3S_6 .

Fig. 2(a) and Fig. 2(b) show the magnetic field dependence of the longitudinal first harmonic voltage $V_{xx}^{3\omega}$ and transverse first harmonic voltage $V_{xy}^{3\omega}$ respectively at different temperatures below T_N with applied a. c. current of 1.74 mA and frequency $f = 13.33$ Hz. The longitudinal $V_{xx}^{3\omega}$ exhibits even symmetry while the transverse $V_{xy}^{3\omega}$ exhibits odd symmetry under positive and negative magnetic fields, which is consistent with the former reports. The magnetic hysteresis phenomenon is originated from its ferromagnetic order under out-of-plane high magnetic field below the T_N . However, the amplitude of third harmonic voltage $V_{xx}^{3\omega}$ decreases as the magnetic field increases, as shown in Fig. 2(c), which is different from first harmonic voltage. Fig. 2(d) shows the odd symmetry properties of $V_{xx}^{3\omega}$ change with magnetic field, and the coercive field increases as the temperature decreases. The longitudinal harmonic voltage $V_{xx}^{n\omega}(B)$ was calculated by the formula $V_{xx}^{n\omega}(B) = (V_{xx}^{n\omega}(B) + V_{xx}^{n\omega}(-B)) / 2$ and transverse harmonic voltage $V_{xy}^{n\omega}(B) = (V_{xy}^{n\omega}(B) - V_{xy}^{n\omega}(-B)) / 2$ to exclude the influence of the electrode asymmetry. The initial data of harmonic voltage change with magnetic field is shown in SI.1.

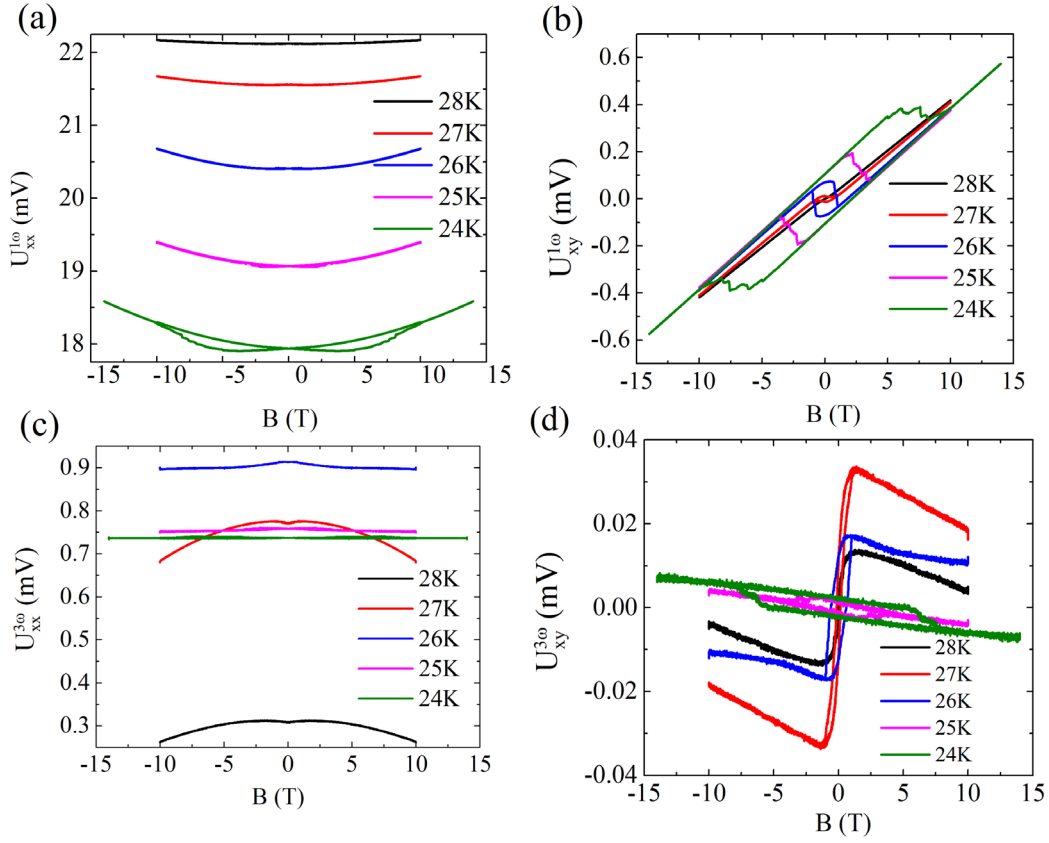


Fig.2. The magnetic field-dependent nonlinear transport properties in CoNb_3S_6 . (a-d) The out-of-plane B-fields dependence of the longitudinal first-harmonic voltage $V_{xx}^{1\omega}$ (a), transverse first harmonic voltage $V_{xy}^{1\omega}$ (b), third-harmonic voltage $V_{xy}^{3\omega}$ (c), transverse third harmonic voltage $V_{xy}^{3\omega}$ (d), measured at different temperatures.

3. The a.c. current amplitude-dependent longitudinal transport properties in CoNb_3S_6 .

Fig. 3(a) shows the a. c. current amplitude-dependent longitudinal first harmonic transport properties at different temperatures in CoNb_3S_6 . The nonlinear first harmonic I-V behavior was observed below the AFM transition $T_N \sim 29$ K as shown in Fig. 3(a). There was no hysteresis for I-V curves sweeping forward and backward, thus can exclude the influence of thermal effect (Fig. S2). Interestingly, the

longitudinal third harmonic voltage $V_{xx}^{3\omega}$ varies with the amplitude of the a. c. current, accompany by a strange transition, as shown in Figure 3(b).

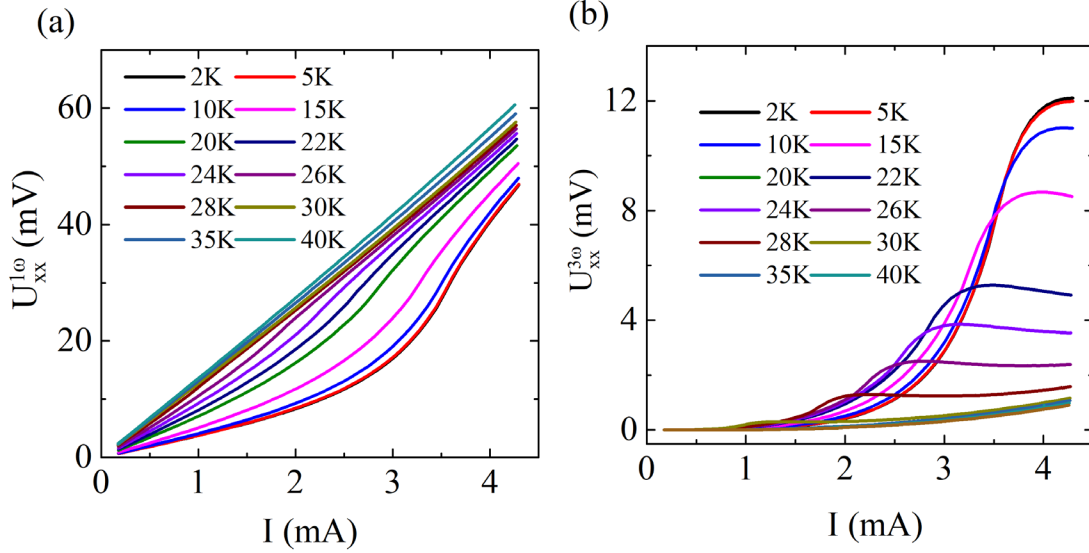


Fig. 3. The a. c. current amplitude-dependent longitudinal transport properties in CoNb₃S₆. (a-b) The amplitude of a. c. current dependence of the longitudinal first harmonic voltage $V_{xy}^{1\omega}$ (a) and third-harmonic voltage $V_{xy}^{3\omega}$ (b) at different temperature with zero magnetic field.

4. The temperature-dependent longitudinal nonlinear transport properties in CoNb₃S₆.

Fig. 4(a) shows the temperature-dependent longitudinal first-harmonic transport properties with different amplitude of a. c. current in CoNb₃S₆. As we can see, the transition temperature (T_N) decreases and the curves of $V_{xx}^{1\omega} - T$ become smoothly as the amplitude of a. c. current increases. The amplitude of longitudinal first harmonic voltage $V_{xx}^{1\omega}$ increases as the amplitude of a. c. current increases, which is consistent with the results of third-harmonic voltage $V_{xx}^{3\omega}$ shown in Fig. 3(b). Interestingly, the third-harmonic voltage $V_{xx}^{3\omega}$ doesn't show an obvious decreasing behaviour during the

cooling process under high a. c. current amplitude (i.e. 4.35 mA). And the $V_{xx}^{3\omega}$ can reach 12 mV as the temperature decreases to 2 K with a. c. current of 4.35 mA.

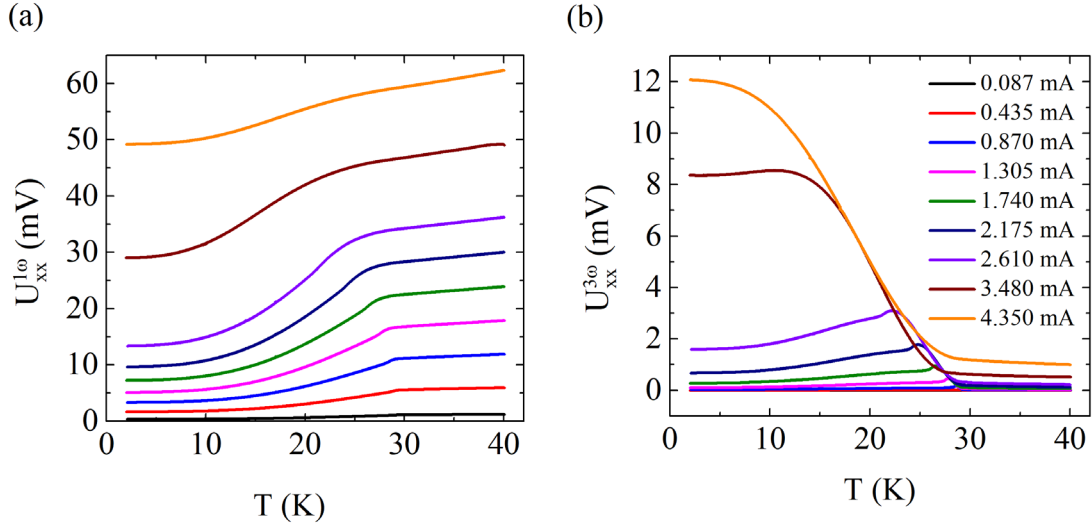


Fig.4. The temperature-dependent longitudinal nonlinear transport properties in CoNb₃S₆. (a-b) Temperature dependence of the $V_{xy}^{1\omega}$ (a) and $V_{xy}^{3\omega}$ (b) at different amplitude of a. c. current with zero magnetic field.

Discussion

The third harmonic nonlinear transport was largely enhanced at AFM transition temperature which is probably connected to its magnetic quadrupoles or the quantum geometrical quadrupoles. The magnetic field dependence of even symmetry $V_{xx}^{3\omega}$ and odd symmetry $V_{xy}^{3\omega}$ at different temperature probably induced by the quantum geometry quadrupoles effect, skew scattering or side jump effect. The origin of the third harmonic nonlinear transport needs further calculations. Besides, the nonlinear first harmonic I-V behaviour have been observed below the AFM transition ($T_N \sim 29$ K) which was probably induced by CDW transition, which is similar as its sister material FeNb₃S₆. The AFM transition temperature (T_N) decreases as the amplitude of a. c. current

increases and the curves of $V_{xx}^{1\omega} - T$ become smoothly at AFM transition, which the large current suppress the AFM order probably. Also, the third harmonic transport is influenced by the similar effect.

Conclusion

In summary, we measured the third order nonlinear longitudinal $V_{xx}^{3\omega}$ and transverse $V_{xy}^{3\omega}$ in topological chiral antiferromagnetic semimetal CoNb_3S_6 . We observed the third order nonlinear longitudinal $V_{xx}^{3\omega}$ increases significantly as the temperature decreases near the AFM transition temperature T_N . Besides, the third harmonic nonlinear transverse $V_{xy}^{3\omega}$ varied with magnetic field with a loop which is consistent with its first harmonic anomalous hall effect. The magnetic field dependence of even symmetry $V_{xx}^{3\omega}$ and odd symmetry $V_{xy}^{3\omega}$ under different temperature probably induced by the quantum geometry quadrupoles effect. The first order I-V curve behave nonlinear characteristic was observed below the Neel temperature T_N , which is possibly corresponded to a gap which induced by the possible CDW order with an antiferromagnetic order transition. At the same time, the third harmonic nonlinear longitudinal $V_{xx}^{3\omega} - T$ curve has two plateau as the amplitude of current increases, which is connected to the CDW state. Our study opens the door to explore the origin of third harmonic nonlinear and interaction with AFM and CDW orders.

Methods

Materials Synthesis

CoNb₃S₆ single crystals were synthesized by chemical vapor transport (CVT) method. Firstly, polycrystalline CoNb₃S₆ was prepared by heating the mixture of Co, Nb and S powder with a stoichiometric of 1:3:6 at 900 °C for 5 days. Then, 2 g of the powder and 0.75 g/mL iodine were sealed in a quartz tube to grow single crystals with a temperature gradient 950 °C to 850 °C for 10 days. The single-crystal x-ray diffraction (XRD) performed on the PANalytical x-ray diffractometer with a Cu K_{α1}. The atomic composition of single crystal CoNb₃S₆ was checked by the dispersive x-ray spectroscopy (EDS).

Device fabrication

The thin flakes were obtained by the traditional Scotch tape exfoliation method. The hall bar-shaped electrodes were fabricated by standard electron beam lithography and metal deposition (5nm Cr/100 nm Au). The thickness of the thin samples was determined by the atomic force microscopy.

Magnetic and transport property measurements

The magnetic susceptibility is measured on the Quantum Design Magnetic Properties Measurement System (MPMS - 5 T). The transport measurements are performed on a Quantum Design physical property measurement system (QD PPMS-14 T). The a. c. voltage measurements were performed with SR830 using the standard four-point method.

Data Availability

For The data that support the findings of this study are available from the corresponding author upon reasonable request.

References

1. Sodemann I, Fu L. Quantum nonlinear Hall effect induced by Berry curvature dipole in time-reversal invariant materials. *Phys. Rev. Lett.* **115**, 216806 (2015).
2. Ma Q, *et al.* Observation of the nonlinear Hall effect under time-reversal-symmetric conditions. *Nature.* **565**, 337-342 (2019).
3. Kang K, Li T, Sohn E, Shan J, Mak KF. Nonlinear anomalous Hall effect in few-layer WTe₂. *Nat. Mater.* **18**, 324-328 (2019).
4. Kumar D, *et al.* Room-temperature nonlinear Hall effect and wireless radiofrequency rectification in Weyl semimetal TaIrTe₄. *Nat. Nanotechnol.* **16**, 421-425 (2021).
5. Du Z, Lu H-Z, Xie X. Nonlinear hall effects. *Nat. Rev. Phys.* **3**, 744-752 (2021).
6. He P, *et al.* Graphene moiré superlattices with giant quantum nonlinearity of chiral Bloch electrons. *Nat. Nanotechnol.* **17**, 378-383 (2022).
7. Wang C, Gao Y, Xiao D. Intrinsic nonlinear Hall effect in antiferromagnetic tetragonal CuMnAs. *Phys. Rev. Lett.* **127**, 277201 (2021).
8. Godinho J, *et al.* Electrically induced and detected Néel vector reversal in a collinear antiferromagnet. *Nat. Commun.* **9**, 4686 (2018).
9. Gao Y, Yang SA, Niu Q. Field induced positional shift of Bloch electrons and its dynamical implications. *Phys. Rev. Lett.* **112**, 166601 (2014).
10. Isobe H, Xu S-Y, Fu L. High-frequency rectification via chiral Bloch electrons. *Sci. Adv.* **6**, eaay2497 (2020).
11. Provost J, Vallee G. Riemannian structure on manifolds of quantum states. *Commun. Math. Phys.* **76**, 289-301 (1980).
12. Niu C, *et al.* Tunable Chirality-Dependent Nonlinear Electrical Responses in 2D Tellurium. *Nano. Lett.* **23**, 8445-8453 (2023).
13. Jin Z, *et al.* Nonlinear topological magnon spin Hall effect. *Phys. Rev. Lett.* **131**, 166704 (2023).
14. Wang N, *et al.* Nonlinear Hall effect with non-centrosymmetric topological phase in ZrTe₅. *arXiv:220207143*, (2022).

15. Ye X-G, *et al.* Control over Berry Curvature Dipole with Electric Field in WTe_2 . *Phys. Rev. Lett.* **130**, 016301 (2023).
16. Lahiri S, Das K, Culcer D, Agarwal A. Intrinsic nonlinear conductivity induced by the quantum metric dipole. *arXiv:220702178*, (2022).
17. Du Z, Wang C, Lu H-Z, Xie X. Band signatures for strong nonlinear Hall effect in bilayer WTe_2 . *Phys. Rev. Lett.* **121**, 266601 (2018).
18. Lai S, *et al.* Third-order nonlinear Hall effect induced by the Berry-connection polarizability tensor. *Nat. Nanotechnol.* **16**, 869-873 (2021).
19. Nagaosa N, Sinova J, Onoda S, MacDonald AH, Ong NP. Anomalous hall effect. *Rev. Mod. Phys.* **82**, 1539 (2010).
20. Wang C, *et al.* Room-temperature third-order nonlinear Hall effect in Weyl semimetal $TaIrTe_4$. *Natl. Sci. Rev.* **9**, nwac020 (2022).
21. Liu H, *et al.* Berry connection polarizability tensor and third-order Hall effect. *Phys. Rev. B.* **105**, 045118 (2022).
22. Smith TB, Pullasserri L, Srivastava A. Momentum-space gravity from the quantum geometry and entropy of Bloch electrons. *Phys. Rev. Res.* **4**, 013217 (2022).
23. Kaplan D, Holder T, Yan B. Unification of nonlinear anomalous hall effect and nonreciprocal magnetoresistance in metals by the quantum geometry. *arXiv:221117213*, (2022).
24. Wang N, *et al.* Quantum-metric-induced nonlinear transport in a topological antiferromagnet. *Nature.* **621**, 487-492 (2023).
25. Gao A, *et al.* Quantum metric nonlinear Hall effect in a topological antiferromagnetic heterostructure. *Science*, **381**, 181–186 (2023).
26. Xiang L, Zhang C, Wang L, Wang J. Third-order intrinsic anomalous Hall effect with generalized semiclassical theory. *Phys. Rev. B.* **107**, 075411 (2023).
27. Zhu Z, *et al.* Third-order charge transport in a magnetic topological semimetal. *Phys. Rev. B.* **107**, 205120 (2023).
28. Sankar S, *et al.* Observation of the Berry curvature quadrupole induced nonlinear anomalous Hall effect at room temperature. *arXiv:230303274*, (2023).
29. Li H, *et al.* Quantum geometry quadrupole-induced third-order nonlinear transport in

- antiferromagnetic topological insulator MnBi_2Te_4 . *arXiv*: 230712313, (2023).
30. Ghimire NJ, Botana A, Jiang J, Zhang J, Chen Y-S, Mitchell J. Large anomalous Hall effect in the chiral-lattice antiferromagnet CoNb_3S_6 . *Nat. Commun.* **9**, 3280 (2018).
 31. Gu P, *et al.* Probing the Anomalous Hall Transport and Magnetic Reversal of Chiral-Lattice Antiferromagnet $\text{Co}_{1/3}\text{NbS}_2$. *arXiv*:230609616, (2023).
 32. Tenasini G, *et al.* Giant anomalous Hall effect in quasi-two-dimensional layered antiferromagnet $\text{Co}_{1/3}\text{NbS}_2$. *Phys. Rev. Res.* **2**, 023051 (2020).
 33. Tanaka H, *et al.* Large anomalous Hall effect induced by weak ferromagnetism in the noncentrosymmetric antiferromagnet CoNb_3S_6 . *Phys. Rev. B.* **105**, L121102 (2022).
 34. Park H, Heinonen O, Martin I. First-principles study of magnetic states and the anomalous Hall conductivity of MNb_3S_6 (M= Co, Fe, Mn, and Ni). *Phys. Rev. Mater.* **6**, 024201 (2022).
 35. Takagi H, *et al.* Spontaneous topological Hall effect induced by non-coplanar antiferromagnetic order in intercalated van der Waals materials. *Nat. Phys.* **19**, 961–968 (2023).
 36. Wu S, *et al.* Discovery of Charge Order in the Transition Metal Dichalcogenide Fe_xNbS_2 . *Phys. Rev. Lett.* **131**, 186701 (2023).

Acknowledgements

Z.A Xu acknowledges the funding from National Key R&D Program of China (2019YFA0308602) and National Science Foundation of China (11774305), the Innovation program for Quantum Science and Technology (Grant No. 2021ZD0302500), L.J Li acknowledges the funding from National Key R&D Program of China (2019YFA0308602), National Science Foundation of China (11774308) and the Zhejiang Provincial Natural Science Foundation of China (LR20A040002).

Contributions

J.J Mi and J.L Li contributed equally to the work. J.J Mi and S Xu performed the crystal growth,

J.J Mi, J.L Li, S Yu and X.Y F performed the device fabrication and characterization, J.J Mi, M.C Li, H.F Zhu and Z Li performed the electrical/magnetic measurement, J.J Mi, J.L Li, M.C Li, L.J Li and Z.A Xu discussed and commented on the work. J.J Mi, L.J Li and Z.A Xu designed the whole experiments and wrote the manuscript, with contributions from all the authors.